Control of Porosity by Using Isoreticular Zeolitic Imidazolate Frameworks (IRZIFs) as a Template for Porous Carbon Synthesis

ARTICLE *in* CHEMISTRY - A EUROPEAN JOURNAL · SEPTEMBER 2012

Impact Factor: 5.73 · DOI: 10.1002/chem.201200957 · Source: PubMed

3 AUTHORS:

Pradip S Pachfule
CSIR - National Chemical Laboratory, Pune
44 PUBLICATIONS **1,011** CITATIONS
SEE PROFILE

Bishnu Biswal
CSIR - National Chemical Laboratory, Pune
12 PUBLICATIONS **243** CITATIONS
SEE PROFILE

Rahul Banerjee
CSIR - National Chemical Laboratory, Pune
126 PUBLICATIONS **5,853** CITATIONS
SEE PROFILE

CHEMISTRY
A EUROPEAN JOURNAL

FULL PAPER

DOI: 10.1002/chem.201200957

Control of Porosity by Using Isoreticular Zeolitic Imidazolate Frameworks (IRZIFs) as a Template for Porous Carbon Synthesis

Pradip Pachfule, Bishnu P. Biswal, and Rahul Banerjee*[a]

Abstract: Herein, by using isoreticular zeolitic imidazolate frameworks (IRZIFs) as a template, we report the synthesis, morphology, and gas adsorption properties of porous carbon synthesized by a nanocasting method at 1000 °C, in which furfuryl alcohol (FA) was used as a carbon source. By using IRZIFs with variable porosity as templates, we could achieve control over the carbon porosity and H_2 and CO_2 uptake. The resultant microporous carbon C-70, synthesized by using ZIF-70 as the template, is the most porous (Brunauer–Emmett–Teller (BET) surface area 1510 $m^2 g^{-1}$). Carbon C-68, synthesized by using ZIF-68, has moderate porosity (BET surface area 1311 $m^2 g^{-1}$), and C-69, synthesized by using ZIF-69, has the lowest porosity in this series (BET surface area 1171 $m^2 g^{-1}$). The porous carbons C-70, C-68, and C-69, which have graphitic texture, have promising H_2 uptake capacities of 2.37, 2.15, and 1.96 wt%, respectively, at 77 K and 1 atm. Additionally, C-70, C-68, and C-69 show CO_2 uptake capacities of 5.45, 4.98, and 4.54 mmol g^{-1}, respectively, at 273 K and 1 atm. The gas uptake trends shown by C-70, C-68, and C-69 clearly indicate the dependence of carbon porosity on the host template. Moreover, the as-synthesized carbons C-70, C-68, and C-69 show variable conductivity.

Keywords: carbon · hydrogen storage · metal–organic frameworks · microporous materials · zinc

Introduction

Nanostructured porous carbon with a high surface area has attracted much attention due to potential applications in liquid adsorption, gas storage, supercapacitors, carriers for drug delivery, and fuel cells.[1,2] The synthesis of these carbon materials has been achieved by using methods such as chemical vapor deposition (CVD), laser ablation, electric arc techniques, carbonization of polymer aerogels, and templated synthetic procedures.[3] Of these much-employed methods for porous carbon synthesis, nanocasting is an efficient way to prepare porous carbon materials. In this method, sacrificial solid templates, such as mesoporous silicas or aluminosilicates (e.g., MCM-48, SBA-15, HMS, MSU-H, SBA-12, SBA-16), are infiltrated with carbon precursors (e.g., sucrose, furfuryl alcohol, phenol resins, polystyrene, mesophase pitches) and then subjected to carbonization at high temperature and selective removal of the inorganic templates.[4] This approach is advantageous for the synthesis of carbon with a controlled pore texture.[3,4]

Research on metal–organic frameworks (MOFs) has attracted much attention due to their potential applications in gas storage, separation, catalysis, multiferroics, drug delivery, etc.[5] Porous MOFs with periodic spacers, suitable for inclusion of small molecules, can reasonably be used as hard templates for porous carbon synthesis. MOFs can allow the entry and polymerization of soft carbon precursors inside the pores, similar to mesoporous silica and zeolites.[6] In the foremost literature report by Xu et al., in which MOF-5 was used as a template for the synthesis of highly porous carbon by using furfuryl alcohol as carbon precursor.[6a] Further reports by Yamauchi et al. (Al-PCP)[6i] and Xu and co-workers (ZIF-8)[6b] revealed the efficiency of MOFs as templates for carbon synthesis. However, the basic criterion used for selection of MOF templates, such as Al-PCP,[6g,i] ZIF-8,[6j] IRMOF-3, IRMOF-8,[6k] and MOF-5,[6a] is based on the fact that the capacity or porosity of the host material to accommodate carbon precursor molecules, will further result into the formation of porous carbon. In some earlier reports, researchers attempted to gain the control over carbon porosity to some extent by varying the temperature and controlled loadings of soft templates.[6j,i] However, recent reports by Yamauchi et al.[6g] and Park and co-workers[6k] once again show the limitations of these templates to control the resulting carbon porosity, although carbon with outstanding porosity has been produced.

Currently, precise control over the porosity of porous carbon synthesized by nanocasting method, in which MOFs can act as templates, is a desirable research goal that has not been fully explored.[6] Attempts to vary the pore size of nanocarbons by using other inorganic templates have so far resulted in either diverse pore sizes or pore systems with large (>8 nm) pore diameters (mesoporous carbon) and redundant metal impurities.[7] To address the issue of fine con-

[a] P. Pachfule, B. P. Biswal, Dr. R. Banerjee
Physical/Materials Chemistry Division
CSIR-National Chemical Laboratory
Dr. Homi Bhabha Road, Pune 411008 (India)
Fax: (+91) 20-25902636
E-mail: r.banerjee@ncl.res.in

Supporting information for this article is available on the WWW under http://dx.doi.org/10.1002/chem.201200957.

trol of carbon porosity, we report herein the use of isoreticular zeolitic imidazolate frameworks (IRZIFs)[8] with variable pore sizes as templates for porous carbon synthesis by using a nanocasting method. Although several reports exist that explain the synthesis of highly porous carbon (with and without carbon precursors) by using MOFs, none of these procedures have precise control of porosity, H_2 uptake, and CO_2 capture. Additionally, all these reports exclusively demonstrate the synthesis of porous carbon from MOFs but fall short in replicating the porosity of the parent MOF template in the resulting carbon. Herein, for the first time, we demonstrate replication and control of the parent MOF template porosity and H_2 and CO_2 uptake in the resulting porous carbon morphology by using ZIFs with different sized pores. The ZIFs used in this work are ZIF-70 (pore aperture 13.1 Å, pore size 15.9 Å), ZIF-68 (pore aperture 7.7 Å, pore size 10.3 Å), ZIF-69 (pore aperture 4.4 Å, pore size 7.8 Å) as MOF templates with variable pore sizes (hard template).[8] Furfuryl alcohol (FA) was used as the carbon precursor for the resulting carbon (C-70, C-68, and C-69) synthesis because it has molecular dimensions ($8.4 \times 6.4 \times 4.2$ Å) that are comparable with the pore size of the ZIFs used (Figure 1). Although there have been a number of different MOFs used for porous carbon synthesis,[6] it is surprising to note that researchers have used only one ZIF (ZIF-8) as a precursor or template for carbon synthesis.[6j] In our opinion, ZIFs should have been the first choice as a precursor or template for nanocasting method because they possess zeolitic architecture, that is, large pores combined with a narrow pore aperture. Herein, we achieved carbon with porosity that ranged from microporous to mesoporous by tuning the porosity of the host ZIF templates. These carbon morphologies with different pore sizes also show variable levels of conductivity.

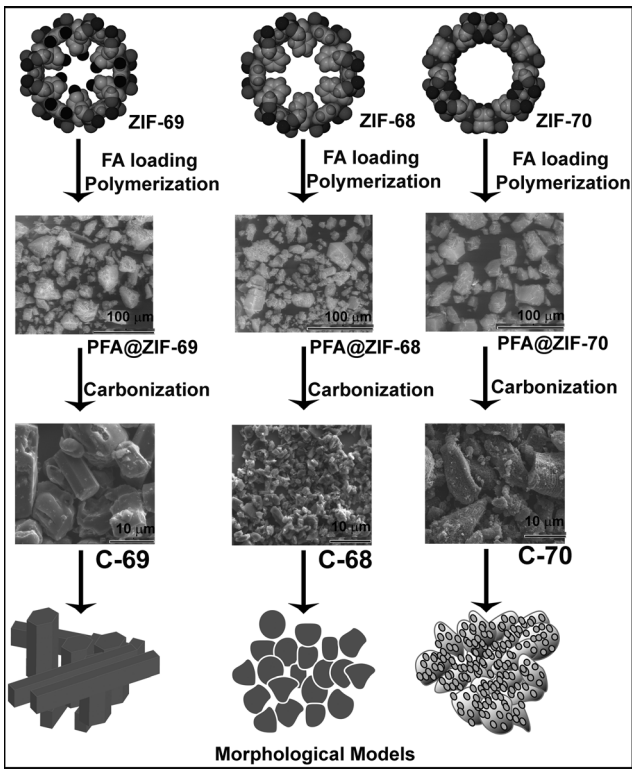

Figure 1. The synthesis of porous carbons C-69, C-68, and C-70 by using ZIF-69, ZIF-68, and ZIF-70 as the MOF template and FA as a carbon source at 1000 °C. The SEM images of the as-obtained PFA@ZIF carbons show that the original ZIF morphology was partially retained in the resulting carbon even after the conversion to carbon. The morphological model provided represents the physical appearance of the carbon obtained.

Results and Discussion

The IRZIF templates used for carbon synthesis are highly porous and synthesized by using heterolinks, which introduce a greater level of complexity into the pore composition and structure, thus impacting the selectivity and multifunctionality of the pores.[8] Moreover, ZIFs, which contains N-based ligands, are more beneficial in the carbon formation than MOFs based on carboxylic acids because the latter produces lower carbon yields as a result of the formation and escape of CO, CO_2, etc., during the carbonization process under an inert gas (N_2/Ar) flow. The highly porous character and robust framework of ZIFs make them suitable as a precursor and a template for porous carbon synthesis. The porosity, particularly the pore diameter of the carbon materials, is a key physical parameter, especially in the adsorption of gases like H_2 and CO_2. To achieve morphologically different carbons with controlled pore sizes, we selected three isoreticular ZIFs, namely, ZIF-70, ZIF-68, and ZIF-69, which have pore sizes of 15.9, 10.3, and 7.8 Å, respectively. Additionally, the ZIFs and MOFs used as the template or carbon source in previous studies have been synthesized by using single linkers (e.g., 2-methylimidazole, 1,4-benzene dicarboxylic acid),[9] whereas ZIF-70, ZIF-68, and ZIF-69[8] were synthesized by using heterolinks (e.g., imidazole, 2-nitroimidazole, benzimidazole, 5-chlorobenzimidazole). The thermal stability and complete removal of the solvent molecules from the pores of evacuated ZIFs (ZIF-70 AE, ZIF-68 AE, and ZIF-69 AE) was confirmed by thermogravimetric analysis (TGA), which shows a long plateau in the temperature range of 150 to 370 °C, which is indicative of the removal of solvent molecules from the framework (Figure S27 in the Supporting Information). The change in surface area with different pore sizes has been confirmed by the Brunauer–Emmett–Teller (BET) surface area, which indicates that ZIF-70, ZIF-68, and ZIF-69 have surface areas of 1637, 1073, and 921 $m^2 g^{-1}$, respectively, which closely matches with the previous reports.[8a] A weighed amount (0.5 g) of evacuated ZIF (ZIF-70 AE, ZIF-68 AE, and ZIF-69 AE) was mixed with a fixed quantity of FA (4.8 g), so that a different amount of FA enters into the pores of ZIFs (FA@ZIFs) depending on the porosity. Further polymerization of these FA molecules inside the ZIFs (PFA@ZIFs; PFA = poly(furfuryl alcohol)) at elevated temperature (150 °C) resulted in the formation of PFA inside the pores

of ZIFs. Because ZIF-70 has the highest surface area and pore size, the amount of FA absorbed inside the pores is highest and the quantity of PFA formed is higher than in ZIF-68 and ZIF-69. Likewise, ZIF-68, which has moderate porosity, accommodates a moderate amount of PFA inside the pores, whereas ZIF-69, which has the lowest porosity, has the least amount of PFA inside the pores. This was confirmed by weight measurements taken after each step (ZIF-70@PFA = 0.612 g; ZIF-68@PFA = 0.586 g, ZIF-69@PFA = 0.577 g). Repeated washing of the FA@ZIFs with aliquots of absolute ethanol restricts the formation of PFA on the outer surface of the ZIFs and selectively allows the formation of PFA inside the pores. The large pores with small pore apertures restrict the escape of FA molecules from the pores while washing and heating during the formation of PFA. The selective formation of PFA inside the pores of ZIFs has been confirmed by SEM analyses of PFA@ZIF-70, PFA@ZIF-68, and PFA@ZIF-69 samples (Figure 1). It is observed that the outer surface of the ZIF crystals are not covered with any polymeric materials, similar to evacuated ZIF samples (Figure 1 and Figures S6, S14, and S22 in the Supporting Information). The increased percentage of atomic oxygen in the samples of PFA@ZIFs compared with evacuated ZIFs, analyzed by using EDAX analyses, again confirms the loading of FA and PFA (see Figures S6, S14, and S22 and the discussion in Section S5 in the Supporting Information). To show the extent of loading of PFA in the pores of ZIFs, we performed a surface area analysis for PFA@ZIF-70, PFA@ZIF-68 and PFA@ZIF-69, as shown in Figure 4a made this an x code. From this analysis it was clear that, due to the loading of PFA inside the pores of ZIFs, the surface area of these PFA-loaded ZIFs (PFA@ZIF-70 = 119 $m^2 g^{-1}$; PFA@ZIF-68 = 39 $m^2 g^{-1}$, PFA@ZIF-769 = 23 $m^2 g^{-1}$) decreases to a significant extent compared with ZIF-70 AE (1730 $m^2 g^{-1}$), ZIF-68 AE (1090 $m^2 g^{-1}$), and ZIF-69 AE (950 $m^2 g^{-1}$). The incorporation of FA and PFA inside the ZIFs was confirmed by IR spectra, in which characteristic peaks for FA and PFA match well with those for FA@ZIF and PFA@ZIF, as shown in Figure 2 (see Sections S2, S4, and S4 in the Supporting Information for more information and discussion on the IR and PXRD of FA- and PFA-loaded ZIFs).

Furthermore, to confirm the loading of the FA and PFA inside the ZIFs without disturbing the ZIF crystallinity, PXRD analysis of these samples were performed. The PXRD analyses confirm that, even after inclusion of FA and formation of PFA inside the pores of ZIFs at higher temperature, the crystallinity of ZIFs remains intact (Figure 2). The additional peaks in the PXRD patterns of FA@ZIFs and PFA@ZIFs compared with evacuated and simulated PXRD patterns of ZIFs suggest the incorporation of FA and PFA inside the pores. The broadening of peaks in the case of PFA@ZIFs could occur as a result of expansion of pores, due to additional stress generated inside due to incorporated FA and PFA or applied temperature during the formation of PFA from FA (150 °C).[10] We performed TGA analyses

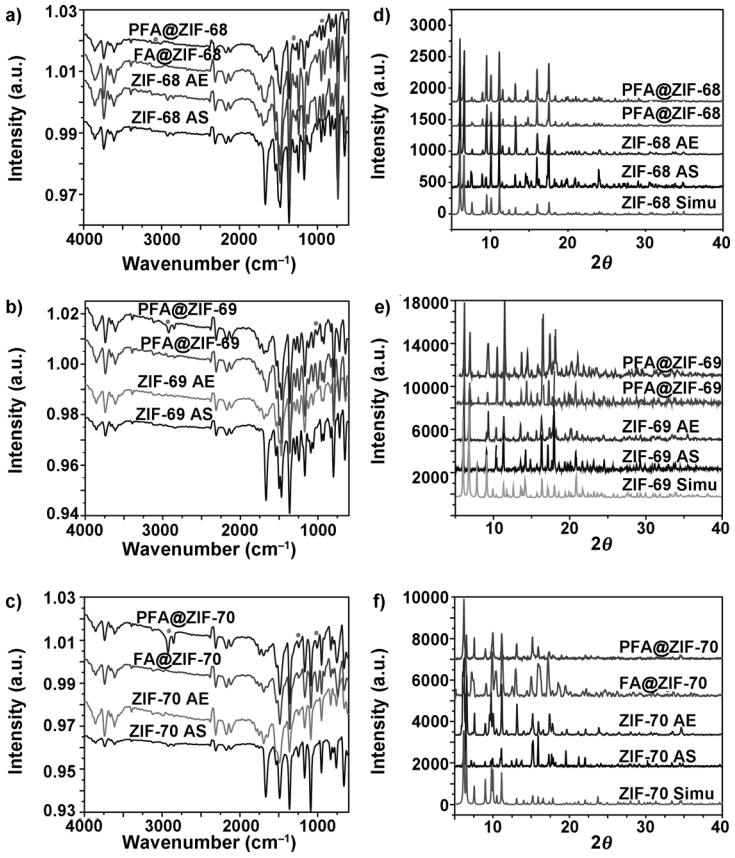

Figure 2. a)–c) The FTIR spectra and d)–f) the PXRD patterns for as-synthesized ZIFs (ZIF AS), ZIFs after evacuation (ZIFs AE), ZIFs after furfuryl alcohol incorporation (FA@ZIFs), and ZIFs after polymerization of FA inside the pores (PFA@ZIFs). In the IR spectra of a) ZIF-68, b) ZIF-69, and c) ZIF-70, the characteristic peaks for FA and PFA are marked. The PXRD patterns of d) ZIF-68, e) ZIF-69, and f) ZIF-70 show the crystallinity of the ZIF samples after each step.

of the FA@ZIF samples (FA@ZIF-70, FA@ZIF-68, FA@ZIF-69) and PFA@ZIF samples (PFA@ZIF-70, PFA@ZIF-68, PFA@ZIF-69) to quantify the loading of FA and PFA inside the ZIFs (See Section S7 in the Supporting Information). The TGA analyses of FA@ZIF-70 shows weight loss of about 25% in the temperature range of 100 to 175 °C due to degradation of FA molecules from the framework; whereas FA@ZIF-68 and FA@ZIF-68 show weight losses of about 18 and 15% over a similar temperature range, respectively, which match well with loading percentage calculated by using weights of PFA@ZIF and ZIFs AE (Figure S28 in the Supporting Information). The TGA analyses of PFA@ZIFs show inconsistent weight loss over a large temperature range from 100 to 400 °C due to the decomposition of PFA from the framework over the whole temperature range (Figure S29 in the Supporting Information). The discrete change in the TGA traces of FA@ZIFs and PFA@ZIFs substantiates the formation of PFA from the FA inside the pores of ZIFs at elevated temperature and reduced pressure (See Section S7 in the Supporting Information).

The ZIFs loaded with PFA inside the pores (PFA@ZIF-70, PFA@ZIF-68, PFA@ZIF-69) were subjected to carbonization at 950 °C for 3 h with a heating rate of 5 °C min^{-1} under an argon atmosphere to form porous carbons (C-70, C-68, C-69). In previous reports, temperatures of less than 900 °C have been used for the carbonization of MOFs, but these conditions result in the formation of metal oxide nanoparticles embedded into the carbon matrix.[6a,i] To acquire phase-pure carbon, washing of these materials with strong acids, such as HF and HCl, becomes necessary. To avoid the additional step of washing carbon with acid solutions, a temperature of 1000 °C, which is much higher than the boiling point of metallic zinc (908 °C), was used so that Zn vaporized in the stream of flowing argon gas and left the carbon matrix. To further confirm the removal of Zn from the carbon formed, we performed an EDAX analysis that shows that the percentage of Zn present in the carbon matrix is almost negligible (that is, less than <1% in all cases; see Figures S7, S15, and S23 in the Supporting Information). Because the ZIFs used in this study have relatively low framework densities (ZIF-70 = 0.885 mg m^{-3}, ZIF-68 = 1.047 mg m^{-3}, ZIF-69 = 1.295 mg m^{-3}), the yields of the resulting carbon materials are moderate and depend on the amount of PFA present inside the pores of the ZIFs. The quantification of the exact amount of porous carbon obtained from pyrolysis of PFA@ZIF-70, PFA@ZIF-68, and PFA@ZIF-69 is difficult because the carbon formed has low density and the chances of losing tiny carbon particles from the furnace tube under the argon flow are high. As mentioned above, although ZIF-70 has the lowest framework density, the carbonization of PFA@ZIF-70 yields approximately 25.2% carbon (C-70) due to the higher loading of PFA. Similarly, ZIF-68 has a moderate loading of PFA and framework density and gives a yield of about 23.9% carbon (C-68) after carbonization of PFA@ZIF-68. The carbonization of PFA@ZIF-69 gives a similar amount of carbon C-69 ($\approx$24.1%) because ZIF-69 has a higher framework density although its loading of PFA is much lower. The direct carbonization of ZIF-70, ZIF-68, and ZIF-69 give yields of 14.1, 16.2, and 16.9% carbon (CZIF-70, CZIF-68 and CZIF-69), respectively, which validates the role of soft template loading to increase the yields.

To authenticate the morphology of the resulting porous carbons and the effect of MOF porosity on the resulting carbon morphology synthesized by using these IRZIFs, we performed SEM and TEM analyses of C-70, C-68, and C-69. From the SEM images of the original ZIFs and the obtained porous carbon materials, it is very clear that the original ZIF morphology was partially retained in the resulting carbon even after the conversion (see Figure 1 and Figures S7, S15, and S23 in the Supporting Information). In the case of C-68, aggregation of carbon particles in the form of blocks 5 to 10 μm in size was observed, whereas C-69 shows highly ordered, cylindrical, block structures about 7 × 15 μm in size. The SEM images of C-70 shows a sponge-like morphology with 1 to 2 μm holes on the outer surface of the carbon lumps, which gives an idea about the porous nature of C-70 (Figure 1 and Figure S23 in the Supporting Information). The TEM images clearly show oriented multilayer domains and a few indistinguishable graphene sheets stacked in parallel positions. As shown in previous reports,[6j,i] disordered graphene layer domains were mostly observed for C-70, C-69, and C-68 in all samples, which was further confirmed by PXRD patterns and Raman spectra. Also, voids with few nm in size were formed by a few carbon layers, although their arrangements were disordered and could not be observed clearly in the TEM images (Figure 3 and Figures S8, S16, and S24 in the Supporting Information). In the most porous C-70, distinct micro-holes a few nm in size were observed to be distributed over the entire area, whereas C-68 also has a similar texture with comparatively smaller micro-holes. However, in C-69, which has lower porosity than C-68 and C-70, these micro-holes are absent. We can infer from the aforementioned observations that the morphology and porosity of the resultant carbon materials could be tuned by changing the template porosity (Figure 3).

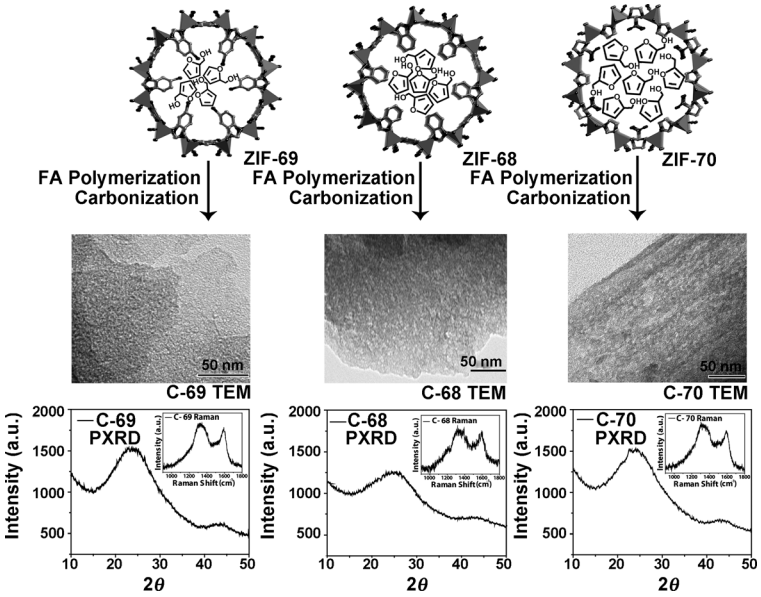

Figure 3. Middle: High-magnification bright-field TEM images of as-synthesized C-69, C-68, and C-70 after the carbonization of PFA@ZIF-69, PFA@ZIF-68, and PFA@ZIF-70, respectively. Bottom: PXRD patterns of as-synthesized C-69, C-68, and C-70, showing characteristic peaks for carbon. Insets: Raman shifts for C-69, C-68, and C-70 show characteristic peaks for graphitic carbon.

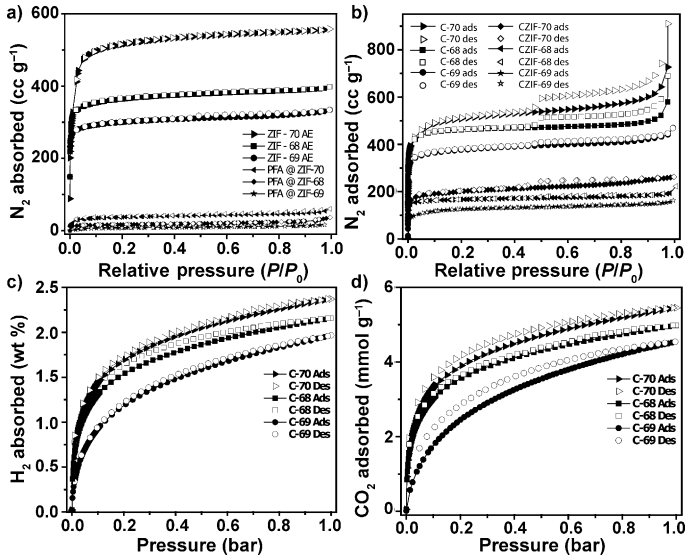

Figure 4. Gas adsorption analyses of ZIFs AE, PFA@ZIFs and the porous carbons. a) N_2 adsorption isotherms for ZIFs after evacuation and PFA@-ZIFs at 77 K and 1.01 atm (1 bar). b) N_2 adsorption isotherms for as-synthesized C-70, C-68, and C-69 and for CZIF-70, CZIF-68, and CZIF-69 at 77 K and 1.01 atm (1 bar). c) H_2 adsorption isotherms for as-synthesized C-70, C-68, and C-69 at 77 K and 1.01 atm (1 bar). d) CO_2 adsorption isotherms for as-synthesized C-70, C-68, and C-69 at 273 K and 1.019 atm (1 bar). C-70 and ZIF-70 AE: filled and open triangles; C-68 and ZIF-68 AE: filled and open squares; C-69 and ZIF-69 AE: filled and open circles. Filled and open symbols represent adsorption and desorption branches for each isotherm, respectively.

Furthermore, we performed PXRD analyses of the carbons obtained to validate their graphitic nature and the presence or absence of impurities in the carbon matrix. The PXRD patterns of C-70, C-69, and C-68 show two broad peaks at $2\theta \approx 25$ and 44°, which correspond to the typical characteristic peaks of graphitic carbon (002) and (101) diffractions (Figure 3 and Section S6 in the Supporting Information).[11] The absence of additional peaks in the PXRD pattern of the carbon verifies the absence of the impurities in the carbon matrix. Porous carbon materials C-70, C-69, and C-68 were further analyzed by using Raman spectroscopy to obtain information on their surfaces and topology (see Figures S2, S10, and S18 in the Supporting Information). As shown in Figure 3, the broad peaks at 1338 and 1594 cm^{-1} in the Raman spectra of C-70, C-69, and C-68 correspond to D and G bands, respectively, which represent the defects in the carbon and the vibrational mode of the movement in opposite directions of two carbon atoms in a graphite sheet.[12] The relative intensity (ID/IG) ratios for C-68, C-69, and C-70 carbons are almost the same, although each of these carbon materials shows different surface morphology (Figure S26 in the Supporting Information). This indicates that the degree of graphitization in the carbon morphologies were almost intact despite changes in the templates for synthesis.

Nitrogen adsorption–desorption experiments were performed on as-synthesized samples of C-70, C-68, and C-69 to examine the surface areas of these materials. The isotherms collected at 77 K and 1 atm pressure show typical Type I behavior with a steep increase at low relative pressure, which suggests that a microporous nature dominates (Figure 4b). The small hysteresis of the desorption curves before $P/P_0 = 0.5$ for all the samples indicates the presence of mesopores as well. The activated sample of C-70 exhibits the highest BET and Langmuir surface areas of 1510 and 2342 $m^2 g^{-1}$, whereas C-68 shows BET and Langmuir surface areas of 1311 and 2064 $m^2 g^{-1}$, respectively. The activated sample of C-69 also shows a similar isotherm with lower BET and Langmuir surface areas of 1171 and 1706 $m^2 g^{-1}$. This variation in the surface area for C-70, C-68, and C-69 can be justified because the more porous ZIF-70 templated formation of C-70 has higher surface area, average pore size, and total pore volume, whereas ZIF-68 and ZIF-69, which have lower porosity, template the formation of carbons C-68 and C-69 with lower surface area, pore size, and total pore volume (Table 1). The retention and transfer of

Table 1. Surface area, average pore volume, total pore volume, and H_2 and CO_2 uptake for porous carbons (C-68, C-69, C-70) and ZIFs (ZIF-69, ZIF-68, ZIF-70).[a]

Material	Surface area [$m^2 g^{-1}$] BET	Langmuir	Average pore size [nm]	Total pore volume [$cm^3 g^{-1}$]	H_2 uptake [wt %]	CO_2 uptake [mmol g^{-1}]
C-69	1171	1706	1.208	0.725	1.96	4.54
C-68	1311	2064	1.978	1.381	2.15	4.76
C-70	1510	2342	2.374	1.749	2.37	5.45
ZIF-69[8b]	950	1070	0.72	0.30	–	≈2.90
ZIF-68[8b]	1090	1229	1.02	0.46	–	≈2.98
ZIF-70[8b]	1730	1970	1.59	0.57	–	≈2.32

[a] All reported gas adsorption properties were performed at 1 atm. H_2 adsorption analyses were carried out at 77 K and CO_2 uptake at 273 K. Average pore size has been determined using DFT and Barrett–Joyner–Halenda (BJH) methods. Total pore volume was calculated by using model N_2 adsorption isotherms collected at 77 K on carbon by assuming slit/cylindrical pores and using the QSDFT method.

ZIF porosity into the resulting carbon porosity shows the critical role of these ZIFs as templates for the resulting carbon formation and direct relationship between amount of FA incorporated and carbon porosity.[6i] To further understand the exact role of the FA content on the resulting carbon porosity, we performed surface area analyses (BET and Langmuir) on the carbons CZIF-70, CZIF-68, and CZIF-69 obtained by direct carbonization of the respective ZIFs (ZIF-70 AE, ZIF-68 AE, and ZIF-69 AE) without loading FA in the pores. The analyses on these CZIF-70, CZIF-68, and CZIF-69 samples show BET surface areas of 625, 509, and 423 $m^2 g^{-1}$ (see Figure 4b). The trends observed in the surface area of C-70, C-68, and C-69 have also been observed for CZIF-70, CZIF-68, and CZIF-69, with comparatively low N_2 uptake. These surface area analyses performed on CZIF-70, CZIF-68, and CZIF-69 indicates the importance of the precursor (FA) loading and the template effect

on the resulting carbon content and the porosity because there is a more than twofold increase in the surface area of C-70, C-68, and C-69 compared with CZIF-70, CZIF-68, and CZIF-69 (Table 1).

To obtain further information on the pore size and distribution, we analyzed the N_2 adsorption isotherms of C-70, C-68, and C-69 by using quenched solid density functional theory (QSDFT) methods (see Section S9 in the Supporting Information). As shown in Figure 5a, for sample C-69,

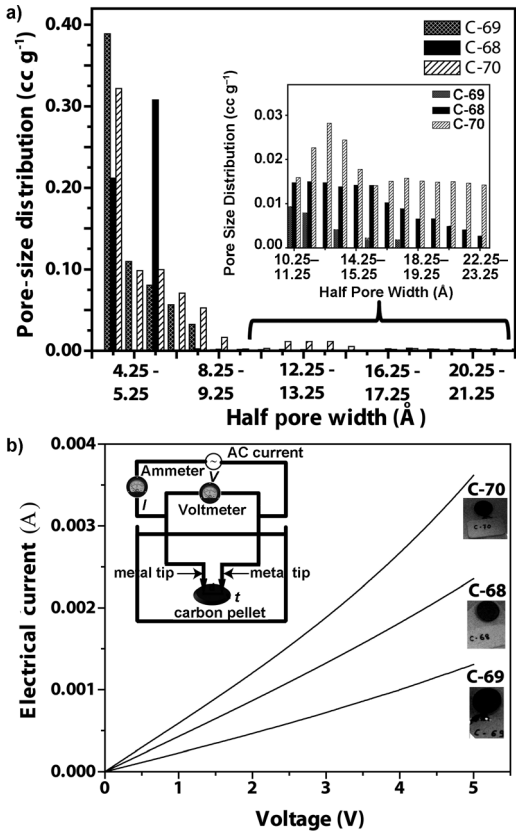

Figure 5. Pore-size distribution and electrical conductivity measurements of C-70, C-68, and C-69. a) Pore-size distributions for C-70, C-68, and C-69 calculated by using a DFT volume histogram method. Inset: The pore-size distribution in the mesoporous region (10.00–25.00 Å). b) Electrical conductivity measurements performed on C-70, C-68, and C-69 by using a two-probe conductivity measurement technique, which shows the conducting performance of the porous carbons. Inset: The circuit diagram is shown; d = distance between two metal tips, t = thickness of carbon pellet.

which has the lowest surface area, most of the pores fall within the diameter range of 7 to 11 Å (micropores) and very few pores are found in the range of 30 to 40 Å diameter (mesopores). In contrast, sample C-70, with the highest surface area, shows fewer pores in the range of 6 to 18 Å (micropores) and more pores in the range of 30 to 40 Å diameter (mesopores), and in sample C-68 the pore-size distribution between micropores (6–14 Å) and mesopores (30–38 Å) is approximately equally distributed over the carbon framework. Similar results were reproduced by using DFT volume histogram plots for C-70, C-68, and C-69 (Figures S33–S35 in the Supporting Information). These results obtained by using DFT show good agreement with the results obtained by using QSDFT and confirm the influence of the surface area of the IRZIFs on the pore-size distribution of C-70, C-68, and C-69 (see Section S9 in the Supporting Information for more plots and information on pore-size distribution).

The overall control over the resulting carbon porosity and texture with comparative surface area encouraged us to carry out H_2 and CO_2 uptake measurements. H_2 (77 K) and CO_2 (273 and 298 K) adsorption isotherms were collected at 1 atm and show typical Type I isotherms that do not exhibit hysteresis, which confirms the reversible uptake of H_2 in the C-70, C-68, and C-69 samples. As shown in Figure 4c, the hydrogen uptake capacities of C-70, C-68, and C-69 are 2.37, 2.15, and 1.96 wt%, respectively, as the pressure approaches 1 atm. The reversible and high H_2 uptake at less than 0.1 atm indicates the high affinity for H_2 adsorption of the porous carbons. As confirmed from the average pore size and total pore volume, the leading micropore distribution could be beneficial for the high H_2 uptake. Similarly, CO_2 uptake measurements performed for the carbons at 273 and 298 K show reversible adsorption, which indicates the inertness of the carbons toward the adsorbates (Figure 4d). At 273 K, C-70, C-68, and C-69 adsorb 5.45, 4.76, and 4.54 mmol g^{-1} CO_2, respectively, as the pressure approaches 1 atm. At elevated temperature (298 K), C-70, C-68, and C-69 adsorb 4.49, 4.00, and 3.86 mmol g^{-1} CO_2, as shown in Figure S32 in the Supporting Information (Table 1). The trends obtained for the surface area of C-70, C-68, and C-69 are also maintained for the H_2 and CO_2 uptake. The H_2 and CO_2 uptakes shown by these materials can be justified because the higher pore volume and average pore size of C-70 adsorbs the most H_2 and CO_2, whereas C-68 adsorbs moderate amounts and C-69 adsorbs the lowest amounts in this series, due to decreasing pore volume and average pore size.

As discussed above, the porous carbons C-70, C-68, and C-69 obtained by the carbonization of PFA@ZIF-70, PFA@ZIF-68, and PFA@ZIF-69 show lower surface areas and pore volumes compared with previously reported carbons, such as NPC,[6a] WMC,[6c] NPC_{530}, NPC_{1000},[6f] MC,[6e] MAC-A,[6e] C800, C-1000,[6j] and MDC-1[6k] (Table 2). However, these carbons have a higher surface area than some reported carbons, such as Al-PCP-FA1, Al-PCP-FA2,[6i] NPC_{650}, NPC_{800},[6f] and MDC-3.[6k] Although C-70, C-68, and C-69 have limited surface area, the hydrogen uptake shown is comparable with previously reported carbons obtained by carbonization of MOFs with or without soft templates. The H_2 uptake shown by C-70 outperforms the hydrogen uptake of C-800 and MDC-8 and is comparable with NPC and C-1000 (Table 2). Although several groups have reported the synthesis of porous carbon by different routes by using MOFs as templates, we were unable to find a report that accounts for the CO_2 uptake of these carbons. Even with limited surface area and pore size, the CO_2 uptake shown by C-70, C-68, and C-69 at 1 atm is promising and higher than

Table 2. Texture parameters and H_2 uptake properties of previously reported porous carbon materials prepared by using MOFs as templates/precursors.

Material	BET surface area $[m^2g^{-1}]$[a]	H_2 uptake [wt %][b]	Ref.	Material	BET surface area $[m^2g^{-1}]$[a]	H_2 uptake [wt %][b]	Ref.
PCP-800	5500	–[c]	[6g]	MC-A	1673	–[c]	[6e]
C1000	3405	2.7	[6j]	NPC_{900}	1647	–[c]	[6f]
AC-K5	3190	–[c]	[6b]	MPC	1543	–[c]	[6e]
MDC-1	3174	3.2	[6k]	NPC_{650}	1521	–[c]	[6f]
NPC_{530}	3040	–[c]	[6f]	C-70	1510	2.3	this work
NPC	2872	2.6	[6a]	KF1-90	1410	–[c]	[6l]
WMC	2587	3.1	[6c]	C-68	1311	2.1	this work
NPC_{1000}	2524	–[c]	[6f]	MPC-A	1271	–[c]	[6e]
HPC	2368	–[c]	[6d]	C-69	1171	1.9	this work
MAC-A	2222	–[c]	[6e]	NPC_{800}	1141	–[c]	[6f]
C800	2169	2.2	[6j]	Al-PCP-FA2	513	–[c]	[6i]
MDC-8	1978	2.4	[6k]	MAC	384	–[c]	[6e]
MC	1812	–[c]	[6e]	Al-PCP-FA1	263	–[c]	[6i]
MDC-3	1678	3.10	[6k]				

[a] The specific surface area was calculated by using the BET method using isotherms collected at 77 K and 1 atm. [b] H_2 adsorption data was collected at 77 K and 1 atm. [c] Either data was not collected or is not represented.

known commercial carbons, such as MAXSORB,[13a,16b] Norit RB2,[13d] and 13X zeolite.[13c,14] The CO_2 uptake shown by these carbons at 298 K and 1 atm outperforms known MOFs, such as MOF-177,[13b] MOF-5,[13b] IRMOF-11,[13b] and MOF-505.[13b,15] Additionally, the CO_2 uptake shown here is comparable to known CO_2-adsorbent MOFs, such as MOF-74[16a] and HKUST-1.[13c] The recently reported carbon molecular sieves (CMSs) VR-5 and VR-93 show similar CO_2 uptake capacity to C-70 at 298 K and 1 atm.[16b]

In the last few years, carbon nanomorphologies have shown potential applications in fields such as electronics and optics due to their unique electrical properties, extraordinary strength, and efficiency in heat conduction. However, due to their high electrical conductivity, these materials have been successfully utilized in the fabrication of electrochemical devices, such as electrochemical actuators and supercapacitors.[18] The huge number of applications of carbon materials in different fields due to their conductivity encouraged us to check the conductivity of carbons C-70, C-68, and C-69. The electrical conductivity of C-70, C-68, and C-69 samples was studied by using a two-probe (copper) method, in which the distance (d) between these metallic tips was kept constant (0.855 cm) to avoid errors in the conductivity (Figure 5b, inset). A weighed amount (0.120 g) of dry C-70, C-68, or C-69 was ground finely with a 20 % solution of Nafion[19] (0.005 g) as a binder and pressurized in a pellet maker with pressure of 15 T to give a pellet of uniform size (radius = 0.5501 cm) and thickness (C-70 = 0.00639 cm, C-68 = 0.00512 cm, C-69 = 0.00627 cm). The pellets obtained were dried under vacuum over overnight (12 h) to remove the traces of moisture present in the pellets (Figure 5b, inset). By maintaining a constant distance between the two copper probes, the electrical conductivity was measured for these samples with varying the applied voltage in the range of 0 to 5 V. The values of increasing voltage (V) versus current (I) obtained were plotted as shown in Figure 5b. A straight line was obtained for C-70, C-68, and C-69 by plotting current (I) versus applied voltage (V), which suggests these carbons have a conducting nature. The conductivity of each particular sample was calculated by using the following equation:

$$\sigma = RA/t$$

in which σ is the electrical conductivity or specific conductance, R is the slope of the straight line obtained by plotting V versus I, A is the area of the pellet ($^1/_2\pi r^2$), and t is the thickness of the pellet.

The conductivity values calculated by using the above equation show higher conductivity for C-70 (0.8311 $S\,cm^{-1}$), whereas C-68 (0.4611 $S\,cm^{-1}$) and C-69 (0.3043 $S\,cm^{-1}$) have very similar conductivity. These carbons with different porosity show variable levels of conductivity, in which the highly porous carbon C-70 with higher pore size shows high electrical conductivity compared with C-68 and C-69. The pellet made from C-69, which has a lower surface area, has the lowest conductivity. Although C-70, C-68, and C-69 show variable conductivity proportional to the porosity of these materials, we were unable to find the exact reason behind these different conductivity values.[20] We are at present attempting to synthesis different carbon morphologies by using the nanocasting method and IRZIFs to understand how the porosity of the precursor as well as carbon morphology affects the conductivity of the product.

Conclusion

We have synthesized porous carbons by using a nanocasting method with IRZIFs as the hard template and furfuryl alcohol as the soft template and carbon precursor. The literature survey suggests that the previously reported methods for porous carbon synthesis have no control over the porosity of the resulting carbon. Some reports show the role of FA and MOF templates in porous carbon synthesis. However, by using a nanocasting method with IRZIFs with different porosity as the hard template and FA as the carbon precursor, we could achieve the direct reproduction of the MOF porosity, H_2/CO_2 uptake, and morphology in the resulting porous

carbons for the first time. The porosity of the ZIF templates have been clearly reproduced and maintained in the resulting carbon. The CO_2 uptake capacities of C-70, C-68, and C-69 at 1 atm and 273 and 298 K outperform most of the commercially available carbons, zeolites, and CMSs. Porous carbons with high CO_2 uptake at room temperature and normal pressure (1 atm) may have applications in CO_2 capture. These carbons show variable levels of conductivity depending on their porosity. Therefore, the obtained carbons with different pore sizes and surface area may indicate a pathway towards energy-related applications, such as supercapacitors and lithium-ion batteries. These carbons may also have future applications in the fields of electrocatalytic synthesis of hydrogen peroxide and the recovery of volatile organic solvents from air or vapor mixtures.

Experimental Section

General procedures: All reagents and solvents for synthesis and analysis are commercially available and were used as received. All experimental operations were performed in air or N_2 and all stock solutions were prepared in *N*,*N*-dimethylformamide (DMF).

Synthesis of zeolitic imidazole frameworks (ZIFs): All three ZIFs used in this study (ZIF-70, ZIF-68, ZIF-69) were synthesized by using a procedure reported in the literature.[8b] The phase purity and crystallinity of the synthesized ZIFs was confirmed by powder X-ray diffraction (PXRD) patterns, which match well with the simulated patterns from single-crystal data, as shown in Figure 2 (see Figures S1, S9, and S17 in the Supporting Information).

Preparation of porous carbon by using ZIFs: To prepare a solvent-free and porous framework, the pale-yellow microcrystals of each ZIF (ZIF-70, ZIF-68, ZIF-69) were soaked in a dry dichloromethane/methanol mixture (1:1) for 12 h. Fresh dry dichloromethane/methanol (1:1) was subsequently added and the crystals were kept in the mixture for an additional 48 h to remove free solvates (DMF) present in the framework. The sample was dried under a dynamic vacuum ($<10^{-6}$ atm) at RT overnight, then heated at 100 °C for 12 h and 120 °C for 12 h under a dynamic vacuum. The framework crystallinity of these ZIFs after evacuation at high temperature and vacuum was confirmed by PXRD at each step (Figure 2 and Sections S2, S3, and S4 in the Supporting Information). A weighed amount (0.50 g) of each evacuated ZIF (ZIF-70 AE, ZIF-68 AE, ZIF-69 AE) was then mixed with furfuryl alcohol (FA; 4.8 g, 0.0489 mmol) with stirring (FA@ZIF). The whole mixture was stirred at RT under a N_2 atmosphere for 24 h to ensure the pores were filled with FA. The N_2 flow was maintained while the ZIF/FA composite mixture was heated at 80 °C for 24 h. To obtain the polymerization of FA inside the pores of ZIFs (PFA@ZIFs), the composite mixture of FA@ZIFs was heated at 150 °C for 8 h under a N_2 atmosphere. To facilitate the removal of FA and PFA molecules adsorbed on the ZIF surfaces in PFA@ZIF composites, each sample was washed a few times with absolute ethanol. From previous reports it was clear that the increased loading of FA inside the templates improves the yield of the resulting carbon and also porosity. To obtain a higher loading of FA inside the ZIF pores, the same PFA@ZIF composites were subjected to impregnation with FA followed by a second polymerization process under the same conditions as before. The PFA@ZIF composites were carefully filtered and washed with ethanol several times to remove FA physically adsorbed on the surface. Due to the different pore sizes of the ZIFs, the weight of the PFA@ZIF composites (PFA@ZIF-70, PFA@ZIF-68, and PFA@ZIF-69 for ZIF-70, ZIF-68, and ZIF-69, respectively) was different (ZIF-70 = 0.612 g, ZIF-68 = 0.586 g, ZIF-69 = 0.577 g). The different roughly calculated loadings of PFA are 22, 17, and 15.5 % for ZIF-70, ZIF-68, and ZIF-69, respectively, which reflects the dependence of incorporation of PFA inside the ZIF pores on the pore size of the bare ZIF (see Sections S2, S3, and S4 in the Supporting Information).

Next, the as-obtained ZIFs with quantitatively different loadings of PFA were subjected to carbonization at 1000 °C for 3 h with a heating rate of 5 °C min^{-1} under an argon atmosphere in a silica container. The carbonization temperature was held at 1000 °C for 3 h under a stream of argon to remove metallic zinc (the boiling point of zinc metal is 907 °C). Finally, the carbon obtained after pyrolysis of PFA@ZIF-70 (C-70), PFA@ZIF-68 (C-68), and PFA@ZIF-69 (C-69) was collected and activated at 250 °C for 24 h to remove trapped water molecules prior to other analyses. To determine the exact role of the FA template on the resulting carbon morphology, yield, and porosity, carbon samples CZIF-70, CZIF-68, and CZIF-69 was obtained by direct carbonization of evacuated ZIF-70, ZIF-68, and ZIF-69 at 1000 °C under an argon atmosphere without loading of any template. The complete removal of zinc from the acquired carbon was confirmed by using an energy-dispersive X-ray spectroscope (EDX) attached to a SEM machine (Figures S7, S15, and S23 in the Supporting Information).

Gas adsorption and pore-size distribution measurements: Low-pressure volumetric gas adsorption measurements for H_2 and N_2 were performed at 77 K, maintained by a liquid nitrogen bath, with pressures ranging from 0 to 1 atm by using an Autosorb-iQ automatic volumetric instrument. CO_2 adsorption measurements were performed at RT (298 K) and 273 K at the same pressure range by using a Quantachrome Quadrasorb automatic volumetric instrument. In all the adsorption measurements, ultra-high-purity H_2 was obtained by using calcium aluminosilicate adsorbents to remove trace amounts of water and other impurities before introduction into the system. The colorless microcrystals of each ZIF sample were soaked in dry dichloromethane/methanol (1:1) for 12 h. Fresh dry dichloromethane/methanol (1:1) was subsequently added and the crystals were kept in the mixture for an additional 48 h to remove free solvates (DMF) present in the framework. The samples were dried under a dynamic vacuum ($<10^{-6}$ atm) at RT overnight, followed by heating at 100 °C for 12 h and 120 °C for 12 h under a dynamic vacuum. The completely dried samples (0.050 g) were loaded into sample cells for a gas adsorption study. Upon heating, ZIF-70, ZIF-68, and ZIF-69 also retain their frameworks (Figure 2), which was confirmed by PXRD patterns. The as-synthesized samples prepared by inclusion of PFA into ZIFs, that is, PFA@ZIF-70, PFA@ZIF-69, and PFA@ZIF-68, were used in the N_2 adsorption study without further purification. The dried carbon materials obtained were activated at 250 °C for 24 h to remove trapped water molecules. The pore distribution plots for the C-70, C-68, and C-69 samples were calculated by using QSDFT and DFT methods by using the nitrogen adsorption isotherms obtained at 77 K and 1 atm.

General instrumentation and methods for data collection: PXRD patterns were recorded by using a Phillips PANalytical diffractometer with $Cu_{K\alpha}$ radiation ($\lambda = 1.5406$ Å), with a scan speed of 2° min^{-1} and a step size of 0.02° (2θ). For the PXRD measurements, the dried ZIFs and carbon samples were placed directly on the XRD plates. The Fourier-transform IR (FTIR) spectra were recorded by using a Bruker Optics ALPHA-E spectrometer equipped with a universal Zn-Se ATR accessory in the 4000–600 cm^{-1} region. Thermogravimetric analysis (TGA) experiments were carried out in the temperature range of 20–800 °C by using a SDT Q600 TG-DTA analyzer under a N_2 atmosphere at a heating rate of 10 °C min^{-1}. All Raman spectroscopy measurements were carried out at RT by using an HR 800 Raman spectrophotometer (Jobin–Yvon HORIBA, France) by using monochromatic radiation emitted by a He–Ne laser ($\lambda = 632.8$ nm) operating at 20 mW. The experiment was repeated several times to verify the consistency of the spectra. Transmission electron microscopy was carried out by using a JEOL JEM 1200 EX instrument operated at an accelerating voltage of 200 kV with a resolution of not less than 3–4 nm. Microscopy analysis was performed by using a LEICA Stereoscan 440 scanning electron microscope equipped with a Phoenix energy-dispersive analysis of X-ray (EDAX). The electrical conductivity measurements for the carbon samples were performed by using a Keithley DC/AC Instruments & Systems setup with two copper probes for contact between the cell and the sample (Figure 5b, inset).

The electrical current measurements were performed by applying a voltage range of 0–5 V for each carbon sample.

Acknowledgements

P.P. acknowledges CSIR for a Senior Research Fellowship (SRF) and B.P.B. acknowledges UGC for fellowship support. R.B. acknowledges Dr. S. Pal, Director of NCL, for an in-house project (MLP020626) and the XIth Five Year Plan Project (CSIR; NWP0022-H) and the Clean Coal Technology Project (NWP0021A) for funding. Financial assistance from the DST (SR/S1/IC-22/2009) and the BRNS (2011/37C/44/BRNS) is acknowledged.

[1] a) A. C. Dillon, K. M. Jones, T. A. Bekkedahl, C. H. Kiang, D. S. Bethune, M. J. Heben, *Nature* **1997**, *386*, 377; b) T. Kyotani, *Carbon* **2000**, *38*, 269; c) R. Ryoo, S. H. Joo, M. Kruk, M. Jaroniec, *Adv. Mater.* **2001**, *13*, 677; d) M. Kang, S. H. Yi, H. I. Lee, J. E. Yie, J. M. Kim, *Chem. Commun.* **2002**, 1944; e) Z. Yang, Y. Xia, R. Mokaya, *Adv. Mater.* **2004**, *16*, 727; f) J. Lee, S. Han, T. Hyeon, *J. Mater. Chem.* **2004**, *14*, 478; g) H. F. Yang, D. Y. Zhao, *J. Mater. Chem.* **2005**, *15*, 1217; h) Z. Yang, Y. Xia, R. Mokaya, *J. Am. Chem. Soc.* **2007**, *129*, 1673; i) Y. Xia, G. S. Walker, D. M. Grant, R. Mokaya, *J. Am. Chem. Soc.* **2009**, *131*, 16493; j) Y. Xia, Z. Yang, R. Mokaya, *Nanoscale* **2010**, *2*, 639; k) H. Itoi, H. Nishihara, T. Kogure, T. Kyotani, *J. Am. Chem. Soc.* **2011**, *133*, 1165.

[2] a) S. A. Johnson, E. S. Brigham, P. J. Ollivier, T. E. Mallouk, *Chem. Mater.* **1997**, *9*, 2448; b) S. Flandrois, B. Simon, *Carbon* **1999**, *37*, 165; c) Z. Hu, M. P. Srinivasan, Y. Ni, *Adv. Mater.* **2000**, *12*, 62; d) Z. Ma, T. Kyotani, Z. Liu, O. Terasaki, A. Tomita, *Chem. Mater.* **2001**, *13*, 4413; e) K. Matsuoka, Y. Yamagishi, T. Yamazaki, N. Setoyama, A. Tomita, T. Kyotani, *Carbon* **2005**, *43*, 876; f) P.-X. Hou, T. Yamazakia, H. Orikasa, T. Kyotani, *Carbon* **2005**, *43*, 2624; g) J. Lee, J. Kim, T. Hyeon, *Adv. Mater.* **2006**, *18*, 2073; h) K. M. Thomas, *Catal. Today* **2007**, *120*, 389; i) M. Jordá-Beneyto, F. Suarez-García, D. Lozano-Castello, D. Cazorla-Amoros, A. Linares-Solano, *Carbon* **2007**, *45*, 293; j) R. T. Yang, Y. Wang, *J. Am. Chem. Soc.* **2009**, *131*, 4224; k) H. Nishihara, P.-X. Hou, L.-X. Li, M. Ito, M. Uchiyama, T. Kaburagi, A. Ikura, J. Katamura, T. Kawarada, K. Mizuuchi, T. Kyotani, *J. Phys. Chem. C* **2009**, *113*, 3189; l) B. Hu, K. Wang, L. Wu, S.-H. Yu, M. Antonietti, M.-M. Titirici, *Adv. Mater.* **2010**, *22*, 813.

[3] a) A. Thess, R. Lee, P. Nikolaev, H. Dai, P. Petit, J. Robert, C. Xu, Y. H. Lee, S. G. Kim, A. G. Rinzler, D. T. Colbert, G. E. Scuseria, D. Tomanek, J. E. Fischer, R. E. Smalley, *Science* **1996**, *273*, 483; b) C. Journet, W. K. Maser, P. Bernier, A. Loiseau, M. Lame de La Chapelle, S. Lefrant, P. Deniard, R. Lee, J. E. Fischer, *Nature* **1997**, *388*, 756; c) B. Zheng, C. Lu, G. Gu, A. Makarovski, G. Finkelstein, J. Liu, *Nano Lett.* **2002**, *2*, 895.

[4] a) C. G. Wu, T. Bein, *Science* **1994**, *266*, 1013; b) S. H. Joo, S. J. Choi, I. Oh, J. Kwak, Z. Liu, O. Terasaki, R. Ryoo, *Nature* **2001**, *412*, 169; c) M. Kruk, M. Jaroniec, T.-W. Kim, R. Ryoo, *Chem. Mater.* **2003**, *15*, 2815; d) A. Lu, A. Kiefer, W. Schmidt, F. Schuth, *Chem. Mater.* **2004**, *16*, 100; e) S. Tanaka, N. Nishiyama, Y. Egashira, K. Ueyama, *Chem. Commun.* **2005**, 2125; f) C. Liang, Z. Li, S. Dai, *Angew. Chem.* **2008**, *120*, 3754; *Angew. Chem. Int. Ed.* **2008**, *47*, 3696; g) T.-P. Fellinger, F. Hasché, P. Strasser, M. Antonietti, *J. Am. Chem. Soc.* **2012**, *134*, 4072.

[5] a) M. Hu, J. Reboul, S. Furukawa, L. Radhakrishnan, Y. Zhang, P. Srinivasu, H. Iwai, H. Wang, Y. Nemoto, N. Suzuki, S. Kitagawa, Y. Yamauchi, *Chem. Commun.* **2011**, *47*, 8124; b) G. Férey, C. Serre, T. Devic, G. Maurin, H. Jobic, P. L. Llewellyn, G. D. Weireld, A. Vimont, M. Daturi, J.-S. Chang, *Chem. Soc. Rev.* **2011**, *40*, 550; c) K. Sumida, D. L. Rogow, J. A. Mason, T. M. McDonald, E. D. Bloch, Z. R. Herm, T.-H. Bae, J. R. Long, *Chem. Rev.* **2012**, *112*, 724; d) M. P. Suh, H. J. Park, T. K. Prasad, D.-W. Lim, *Chem. Rev.* **2012**, *112*, 782; e) J.-R. Li, J. Sculley, H.-C. Zhou, *Chem. Rev.* **2012**, *112*, 869; f) A. Bétard, R. A. Fischer, *Chem. Rev.* **2012**, *112*, 1055; g) C. Wang, T. Zhang, W. Lin, *Chem. Rev.* **2012**, *112*, 1084; h) L. E. Kreno, K. Leong, O. K. Farha, M. Allendorf, R. P. Van Duyne, J. T. Hupp, *Chem. Rev.* **2012**, *112*, 1105; i) Y. Cui, Y. Yue, G. Qian, B. Chen, *Chem. Rev.* **2012**, *112*, 1126; j) M. Yoon, R. Srirambalaji, K. Kim, *Chem. Rev.* **2012**, *112*, 1196; k) P. Horcajada, R. Gref, T. Baati, P. K. Allan, G. Maurin, P. Couvreur, G. Férey, R. E. Morris, C. Serre, *Chem. Rev.* **2012**, *112*, 1232; l) M. O'Keeffe, O. M. Yaghi, *Chem. Rev.* **2012**, *112*, 675; m) R. B. Getman, Y.-S. Bae, C. E. Wilmer, R. Q. Snurr, *Chem. Rev.* **2012**, *112*, 703.

[6] a) B. Liu, H. Shioyama, T. Akita, Q. Xu, *J. Am. Chem. Soc.* **2008**, *130*, 5390; b) H. Wang, Q. Gao, J. Hu, *J. Am. Chem. Soc.* **2009**, *131*, 7016; c) D. Yuan, J. Chen, S. Tan, N. Xia, Y. Liu, *Electrochem. Commun.* **2009**, *11*, 1191; d) H. Deng, S. Jin, L. Zhan, Y. Wang, S. Qiao, L. Tang, X. Liang, W. Qiao, L. Ling, *Mater. Lett.* **2010**, *64*, 1187; e) J. Hu, H. Wang, Q. Gao, H. Guo, *Carbon* **2010**, *48*, 3599; f) B. Liu, H. Shioyama, H.-L. Jiang, X.-B. Zhang, Q. Xu, *Carbon* **2010**, *48*, 456; g) M. Hu, J. Reboul, S. Furukawa, N. L. Torad, Q. Ji, P. Srinivasu, K. Ariga, S. Kitagawa, Y. Yamauchi, *J. Am. Chem. Soc.* **2011**, *133*, 2864; h) R. Das, P. Pachfule, R. Banerjee, P. Poddar, *Nanoscale* **2012**, *4*, 591; i) L. Radhakrishnan, J. Reboul, S. Furukawa, P. Srinivasu, S. Kitagawa, Y. Yamauchi, *Chem. Mater.* **2011**, *23*, 1225; j) H.-L. Jiang, B. Liu, Y.-Q. Lan, K. Kuratani, T. Akita, H. Shioyama, F. Zong, Q. Xu, *J. Am. Chem. Soc.* **2011**, *133*, 11854; k) S. J. Yang, T. Kim, J. H. Im, Y. S. Kim, K. Lee, H. Jung, C. R. Park, *Chem. Mater.* **2012**, *24*, 464; l) Y. Lv, F. Zhang, Y. Dou, Y. Zhai, J. Wang, H. Liu, Y. Xia, B. Tu, D. Zhao, *J. Mater. Chem.* **2012**, *22*, 93.

[7] a) J. S. Lee, S. H. Joo, R. Ryoo, *J. Am. Chem. Soc.* **2002**, *124*, 1156; b) C. Yu, J. Fan, B. Tian, D. Zhao, G. D. Stucky, *Adv. Mater.* **2002**, *14*, 1742; c) C. Yu, J. Fan, B. Tian, F. Zhang, G. D. Stucky, D. Zhao, *Stud. Surf. Sci. Catal.* **2003**, *146*, 45; d) A.-H. Lu, W. Schmidt, B. Spliethoff, F. Schueth, *Adv. Mater.* **2003**, *15*, 1602; e) A. Vinu, K. Ariga, *Chem. Lett.* **2005**, *34*, 674; f) A. H. Lu, W. C. Li, W. Schmidt, F. Schuth, *Microporous Mesoporous Mater.* **2005**, *80*, 117.

[8] a) R. Banerjee, A. Phan, B. Wang, C. Knobler, H. Furukawa, M. O'Keeffe, O. M. Yaghi, *Science* **2008**, *319*, 939; b) R. Banerjee, H. Furukawa, D. Britt, C. Knobler, M. O'Keeffe, O. M. Yaghi, *J. Am. Chem. Soc.* **2009**, *131*, 3875.

[9] a) M. Eddaoudi, J. Kim, N. Rosi, D. Vodak, J. Wachter, M. O'Keeffe, O. M. Yaghi, *Science* **2002**, *295*, 469; b) A. Comotti, S. Bracco, P. Sozzani, S. Horike, R. Matsuda, J. Chen, M. Takata, Y. Kubota, S. Kitagawa, *J. Am. Chem. Soc.* **2008**, *130*, 13664; c) D. Britt, H. Furukawa, B. Wang, T. G. Glover, O. M. Yaghi, *Proc. Natl. Acad. Sci. USA* **2006**, *103*, 10186.

[10] H. Hayashi, A. P. Côte, H. Furukawa, M. O'Keeffe, O. M. Yaghi, *Nat. Mater.* **2007**, *6*, 501.

[11] a) N. Bozovic, I. Bozovic, J. Misewich, *Nano Lett.* **2008**, *8*, 4477; b) K. L. Saenger, J. C. Tsang, A. A. Bol, J. O. Chu, A. Grill, *Appl. Phys. Lett.* **2010**, *96*, 153105.

[12] a) Y. Wang, D. C. Alsmeyer, R. L. McCreery, *Chem. Mater.* **1990**, *2*, 557; b) M. S. Dresselhaus, G. Dresselhaus, R. Saito, A. Jorio, *Phys. Rep.* **2005**, *409*, 47; c) C. N. R. Rao, K. Biswas, K. S. Subrahmanyam, A. Govindaraj, *J. Mater. Chem.* **2009**, *19*, 2457; d) M. S. Dresselhaus, A. Jorio, M. Hofmann, G. Dresselhaus, R. Saito, *Nano Lett.* **2010**, *10*, 751.

[13] a) S. Himeno, T. Komatsu, S. Fujita, *J. Chem. Eng. Data* **2005**, *50*, 369; b) A. R. Millward, O. M. Yaghi, *J. Am. Chem. Soc.* **2005**, *127*, 17998V; c) Z. Liang, M. Marshall, A. L. Chaffee, *Energy Fuels* **2009**, *23*, 2785; d) V. Goetz, O. Pupier, A. Guillot, *Adsorption* **2006**, *12*, 55.

[14] D. M. D'Alessandro, B. Smit, J. R. Long, *Angew. Chem.* **2010**, *122*, 6194; *Angew. Chem. Int. Ed.* **2010**, *49*, 6058.

[15] a) J. Liu, P. K. Thallapally, B. P. McGrail, D. R. Brown, J. Liu, *Chem. Soc. Rev.* **2012**, *41*, 2308; b) S. Ma, H.-C. Zhou, *Chem. Commun.* **2010**, *46*, 44.

[16] a) S. R. Caskey, A. G. Wong-Foy, A. J. Matzger, *J. Am. Chem. Soc.* **2008**, *130*, 10870; b) J. Silvestre-Albero, A. Wahby, A. Sepúlveda-Escribano, M. Martínez-Escandell, K. Kaneko, F. Rodríguez-Reinoso, *Chem. Commun.* **2011**, *47*, 6840.

[17] The low surface area of C-69 compared with C-68 and C-70 can be explained, because C-69 has more pores in the micropore range of 7–11 Å and very few pores in the higher diameter range (mesoporous), which results in less open space for the accommodation of gas molecules. On the other hand, C-68, which has equal pore distributions in both the microporous and mesoporous ranges, has a moderate surface area. Additionally, a larger distribution of pores in the mesoporous region results in the higher surface area of C-70 and results in the availability of more free space for the accommodation of gas molecules.

[18] a) C. Du, J. Yeh, N. Pan, *Nanotechnology* **2005**, *16*, 350; b) A. Kongkanand, R. M. Dominguez, P. V. Kamat, *Nano Lett.* **2007**, *7*, 676; c) R. Jackson, B. Domercq, R. Jian, B. Kippelen, S. Graham, *Adv. Funct. Mater.* **2008**, *18*, 2548.

[19] To make pellets of carbons C-70, C-68, and C-69, 0.005 g of a 20% solution of Nafion was added to the carbon to obtain pellets without cracks or defects. Pellets made without the addition of Nafion do not tolerate the contact of copper tips.

[20] a) T. W. Ebbesen, H. J. Lezec, H. Hiura, J. W. Bennett, H. F. Ghaemi, T. Thio, *Nature* **1996**, *382*, 54; b) E. Raymundo-Piñero, F. Leroux, F. Béguin, *Adv. Mater.* **2006**, *18*, 1877; c) E. Frackowiak, *Phys. Chem. Chem. Phys.* **2007**, *9*, 1774.

Received: March 21, 2012
Revised: May 5, 2012
Published online: ■■ ▮▮, 0000

Pore over this: The control over pore size of porous carbons C-70, C-68, and C-69, synthesized by using a nanocasting method, has been achieved by using isoreticular zeolitic imidazolate frameworks (IRZIFs; ZIF-70, ZIF-68, ZIF-69, see figure) as templates with variable porosity and furfuryl alcohol as the carbon precursor. The porosity of the ZIF templates has been clearly retained in the resulting C-70, C-68, and C-69 structures.

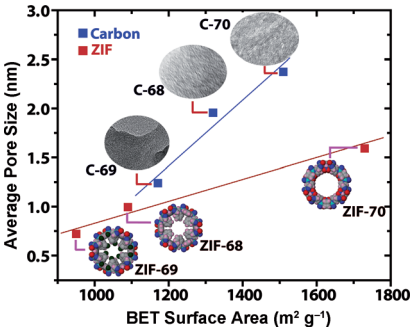

Porous Materials

*P. Pachfule, B. P. Biswal, R. Banerjee** ..... ▮▮▮▮–▮▮▮▮

Control of Porosity by Using Isoreticular Zeolitic Imidazolate Frameworks (IRZIFs) as a Template for Porous Carbon Synthesis